Volume-shear coupling in a mesoscopic model of amorphous materials

E. A. Jagla
Centro Atómico Bariloche, Instituto Balseiro, Comisión Nacional de Energía Atómica, CNEA, CONICET, UNCUYO, Av. E. Bustillo 9500 (R8402AGP) San Carlos de Bariloche, Río Negro, Argentina

(Received 26 February 2022; accepted 30 June 2022; published 22 July 2022)

We present a two-dimensional mesoscopic model of a yield stress material that includes the possibility of local volume fluctuations coupled to shear in such a way that the shear strength of the material decreases as the local density decreases. The model reproduces a number of effects well known in the phenomenology of this kind of material. In particular, we find that the volume of the sample increases as the deformation rate increases; shear bands are no longer oriented at 45° with respect to the principal axis of the applied stress (as in the absence of volume-shear coupling); and homogeneous deformation becomes unstable at low enough deformation rates if volume-shear coupling is strong enough. We also discuss the effect of this coupling on some out-of-equilibrium configurations, which can be relevant to the study of the shear bands observed in metallic glasses.

DOI: 10.1103/PhysRevE.106.014903

I. INTRODUCTION

Dilatancy [1,2] is a property of granular materials characterized by a volume increase that is observed when the material is forced to shear. Traditionally, dilatancy has been known to play an important role in the mechanics of soils and sands [3–6]. However, dilatancy may be considered as a particular case of the volume-shear coupling phenomena, which are also relevant, for instance, in the physics of yield stress fluids (most of which in fact have some kind of "grains" as elementary constituents) [7–11]. Volume-shear coupling has also been invoked as one important ingredient of the physics of materials failing by the nucleation of shear bands, particularly metallic glasses [12–15]. In fact, in this case there is strong evidence (both experimental and numerical) that expansion occurs within the shear bands (see [13] and reference therein). Yet, as the shear band is a very thin object within the bulk, a global dilatancy effect is typically not observed in these cases.

We investigate here the dilatancy effect and the volume-shear coupling in a mesoscopic model of the yielding transition. Previously [16–18], this model has been applied to situations in which the local density of the system was not considered to play an important role, and actually the possible change of density was not even considered. Here, we study the coupled evolution of local strain and local density, and we address the influence of local density fluctuations on the shearing behavior of the system.

The paper is organized as follows. In the next section, we consider a prototypical one-variable mean-field model of the yielding behavior, and we add to it an additional variable describing density changes. We obtain in this simple model the basic properties of the dilatancy effect, particularly the increase in system volume with the increase of strain rate in the system. Section III presents briefly the spatially extended model and the simulation technique. Then in Sec. IV we show that due to volume-shear coupling, the spatial orientation of plastically deformed regions, or shear bands, in spatially extended models is rotated with respect to the case in which there is no such volumetric effect. The orientation we observe departs from the one predicted by the classical Mohr-Coulomb failure criterion, agreeing instead with the orientation predicted by a recently proposed theory. In Sec. V we show that volume-shear coupling can produce a flowing state in the material in which parts of the sample yield and acquire a lower density, while other parts remain essentially rigid, and with a higher density. While all previously mentioned results correspond to steady-state and reversible situations, in Sec. VI we investigate the important case involving applications of samples prepared by some sort of annealing, which are then submitted to a shear deformation until they fail, typically by nucleating a nonequilibrium shear band, as occurs in metallic glasses. Finally, in Sec. VII we summarize and conclude.

II. COUPLING VOLUME AND SHEAR IN A ONE-SITE MODEL

We start by considering a very simple model with two degrees of freedom (representing the shear and volume state of a sample), and we study the appearance of a dilatancy effect. We take as a starting point the well-known Prandtl-Tomlinson model of friction for the shear degree of freedom e_2 [19]. The model is written as a dynamical evolution equation of the form

$$\lambda \dot{e}_2 = -\frac{dV(e_2)}{de_2} + (\dot{\gamma} t - e_2)k, \tag{1}$$

which describes the situation depicted in Fig. 1. The driving $\dot{\gamma} t$ pulls from the variable e_2 through a spring of stiffness k. Note that this spring represents a crucial part of the material under study, and it does not have to be considered as a part of the measuring device. In addition, e_2 is also affected by the force $f_2(e_2) \equiv -dV/de_2$. In a friction context, f_2 represents the corrugated potential between two surfaces sliding against each other. In a context of yielding, f_2 represents the internal stress that a small portion of the system feels due to its

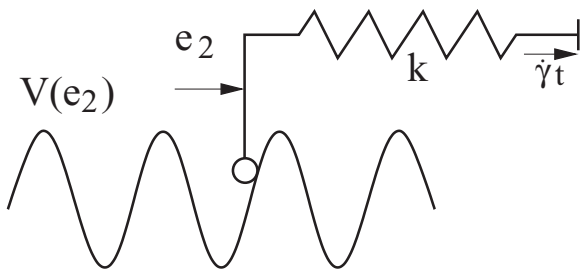

FIG. 1. Schematic representation of the Prandtl-Tomlinson model, mathematically described by Eq. (1).

amorphous nature. In any case, the $f_2(e_2)$ function is expected to have many minima. We will assume here that f_2 is a periodic function. Finally, λ is an effective viscosity coefficient.

In the traditional form of the PT model, the "friction force" is calculated as the average force that the driving has to apply in order to maintain a uniform driving velocity of $\dot{\gamma}$. This force is the one that stretches the spring, so the friction force σ is calculated as

$$\sigma = \langle \dot{\gamma} t - e_2 \rangle k, \tag{2}$$

where the angular brackets notate a temporal average. In the yielding context, an equation like Eq. (1) is taken as a mean-field description of a spatially extended system. In the extended case, $\dot{\gamma} t$ represents the spatial (instantaneous) average of the value of e_2, namely

$$\dot{\gamma} t = \overline{e_2}, \tag{3}$$

and the model equation must be written with the explicit inclusion of the externally applied stress σ in the form

$$\lambda \dot{e}_2 = f_2(e_2) + (\overline{e_2} - e_2)k + \sigma. \tag{4}$$

Spatially averaging this equation, taking into account Eq. (3), we obtain in the yielding context

$$\sigma = \lambda \dot{\gamma} - \overline{f_2}. \tag{5}$$

In any case, the difference between using Eqs. (1) and (2), or (4) and (5), is irrelevant as the difference amounts to a shift in the instantaneous value of e_2 by a constant, which does not alter the main feature of the flow curve (i.e., the $\dot{\gamma}$ versus σ dependence) of the model. In fact, from (2) and (1), an equation similar to (5), namely

$$\sigma = \lambda \dot{\gamma} - \langle f_2 \rangle, \tag{6}$$

is also obtained in the friction context.

We will now extend the PT model to include the possibility of volume fluctuations, described by a variable that is denoted e_1. The value of e_1 will tend to evolve to its stationary value, with a dynamics mainly controlled by the value of the bulk modulus B of the system. Considering an overdamped dynamics, this evolution must be of the form

$$\dot{e}_1 = -B e_1, \tag{7}$$

where the value $e_1 = 0$ was chosen as the equilibrium value. Of course in this trivial form the evolution of e_1 is totally decoupled from the evolution of e_2, and there is no effect of e_1 (that adjusts at $e_1 = 0$ for all values of $\dot{\gamma}$) on e_2.

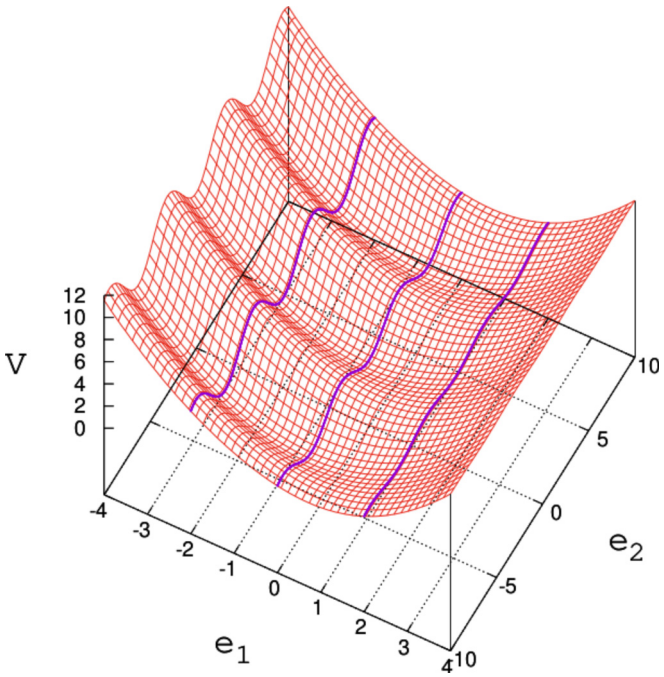

FIG. 2. The potential energy of Eq. (10), for the parameters $B = 1$, $\alpha = 0.4$, and for $U_2(e_2) = 1 - \cos(e_2)$. The blue lines highlight the fact that the corrugation along the e_2 axis decreases (increases) as e_1 increases (decreases).

Now we introduce a coupling between e_1 and e_2 that describes a possible dilatancy effect in the system. We expect that when e_1 increases, the system yields more easily, therefore e_1 must have an effect on the force f_2. So we do the following. We consider a two-dimensional potential energy $V(e_1, e_2)$ from which forces $f_{1,2}$ are obtained as the partial derivatives $f_{1,2} = -\partial V / \partial e_{1,2}$. Therefore, the model equations will be

$$\begin{aligned} \dot{e}_1 &= -\partial V / \partial e_1, \\ \dot{e}_2 &= -\partial V / \partial e_2 + k(\dot{\gamma} t - e_2). \end{aligned} \tag{8}$$

The form of $V(e_1, e_2)$ will dictate the form of the effective coupling between the modes e_1 and e_2. We will use for V the generic form

$$V(e_1, e_2) = \frac{B}{2} e_1^2 + U_1(e_1) U_2(e_2). \tag{9}$$

Note first of all that we isolated the term $B e_1^2/2$ that corresponds to a sample with bulk modulus B. In the second term, $U_2(e_2)$ will be an oscillatory potential with many minima along the e_2 axis. In the case in which the factor $U_1(e_1)$ is a constant, this potential will provide the decoupled model in which e_1 and e_2 evolve separately. However, if the value of $U_1(e_1)$ decreases as e_1 increases, a dilatancy effect will be obtained. We will consider the following form of the potential energy:

$$V(e_1, e_2) = \frac{B}{2} e_1^2 + [1 - \tanh(\alpha e_1)] U_2(e_2). \tag{10}$$

This form (which is plotted in Fig. 2) provides a corrugated potential on e_2 with an amplitude that tends to 0 when e_1

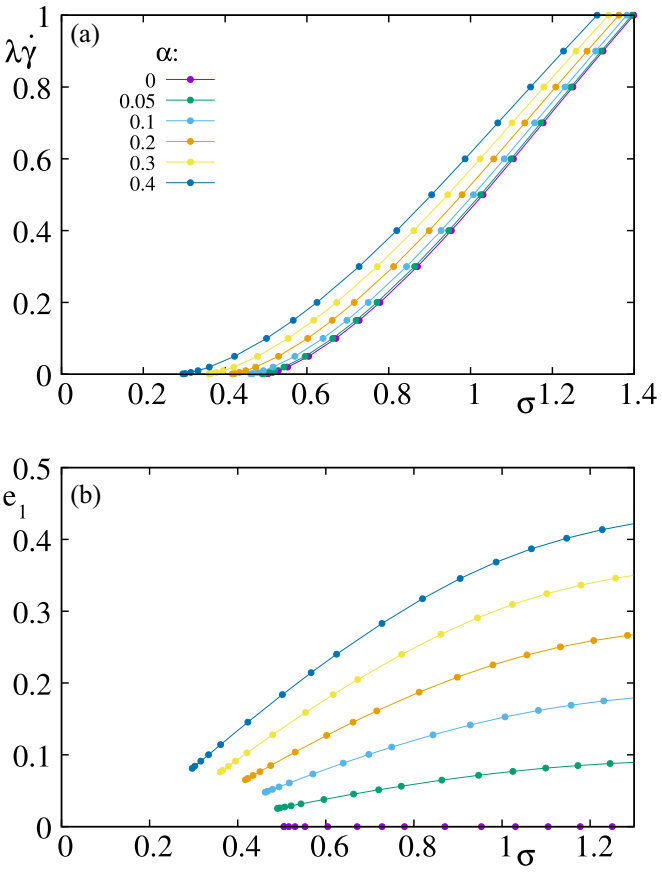

FIG. 3. (a) Flow curves of the one-particle model with coupling between shear and volume degrees of freedom. Different curves correspond to different values of α [Eq. (10)] as indicated. (b) Corresponding curves of the temporal average of the variable e_1 representing the increase in system volume, caused by shear. The volume is larger for larger values of α, and also increases with the value of strain rate $\dot{\gamma}$.

is positive and large (i.e., when the system is very dilated), whereas it saturates to an e_1-independent value for large negative e_1. Therefore, α quantifies the coupling between e_1 and e_2. Coupling vanishes when $\alpha = 0$. The choice of a hyperbolic tangent is made for the sake of concreteness, the quadratic term in e_1 in Eq. (10) will ensure that $\tanh(\alpha e_1) \sim \alpha e_1$ if α is not too large, as will be the case in our results.

In the next section, dealing with an extended system, we will consider some stochastic form of the function U_2. Here, it suffices to consider a single periodic expression that we choose to be of the form

$$U_2(e_2) = 1 - \cos(e_2). \tag{11}$$

Driving along the e_2 direction will produce the effect of modifying the value of e_1. We simulated Eq. (8) using expressions (10) and (11) for the potential and different values of the coupling α. The flow curve $\dot{\gamma}$ as a function of σ and the temporarily averaged values of e_1 are reported in Fig. 3. We see how the volume e_1 increases as $\dot{\gamma}$ (or σ) increases. This is the dilatancy effect. The effect is stronger as the value of α increases. Note also how the flow curve for larger values of α shifts to the left (and in particular the critical stress reduces) at larger α when e_1 is positive.

III. DETAILS ON THE EXTENDED MODEL

The one-site modeling of the previous section is the basis for a spatially extended model in which each site is characterized by its strain and its volume degree of freedom. Full details can be found in the literature [16–18,20]. We concentrate on a two-dimensional system, and we consider the linearized strain tensor ε_{ij} defined in terms of the displacement field u_i,

$$\varepsilon_{ij} = \frac{1}{2}\left(\frac{\partial u_i}{\partial x_j} + \frac{\partial u_j}{\partial x_i}\right), \tag{12}$$

where $i, j = 1, 2$. From here we define one volumetric

$$e_1 \equiv (\varepsilon_{11} + \varepsilon_{22})/2 \tag{13}$$

and two deviatoric strains

$$e_2 \equiv (\varepsilon_{11} - \varepsilon_{22})/2, \tag{14}$$

$$e_3 \equiv \varepsilon_{12}. \tag{15}$$

The deviatoric strains are related by a symmetry rotation of 45°. Overdamped equations of motion are considered for this model, which are obtained by equating the time derivatives of e_i to minus the variation of the total free energy F with respect to e_i. In this process, it has to be taken into account that e_1, e_2, and e_3 are not independent variables, but they are related through [21]

$$Q_1 e_1 + Q_2 e_2 + Q_3 e_3 = 0 \tag{16}$$

with

$$Q_1 \equiv \partial_x^2 + \partial_y^2, \tag{17}$$

$$Q_2 \equiv \partial_y^2 - \partial_x^2, \tag{18}$$

$$Q_3 \equiv -2\partial_x \partial_y. \tag{19}$$

This constraint is the ingredient that generates the well-known long-range elastic Eshelby interaction in the system. Therefore, the equations of motion are written as

$$\lambda \dot{e}_i = -\frac{\partial V}{\partial e_i} + \Lambda Q_i, \tag{20}$$

where

$$\Lambda = -\frac{\sum (f_i Q_i)}{\sum (Q_i^2)} \tag{21}$$

is a Lagrange multiplier adjusted to satisfy the constraint [16–18], and λ is again an effective viscosity coefficient. Volume-shear coupling is obtained with use of a $V(e_1, e_2, e_3)$ function qualitatively similar to that in Eq. (10), but also with some differences due in part to technical reasons. First of all, taking into account that physically e_2 and e_3 differ only by a spatial rotation of 45°, we should consider $(e_2^2 + e_3^2)$ as the variable to couple to e_1 through a parameter α similar to that used in the previous section. However, notice that in our implementation using finite differences on a square lattice, the variables e_1 and e_2 are calculated on the nodes of this lattice,

whereas e_3 is defined at the centers of the plaquettes. This makes a possible coupling between e_1 and e_3 a nonlocal one in the present numerical scheme, producing spurious effects that require special care to be avoided. This is certainly a point that will deserve further attention. However, since we will apply the external driving along the e_2 direction, it may be expected that the main effect we are interested in can be captured by coupling e_1 to e_2 only, leaving e_3 evolving without any coupling to e_1. Therefore, we will model the local potential energy as

$$V(e_1, e_2, e_3) = \frac{B}{2}e_1^2 + [1 - \tanh(\alpha e_1)]U_2(e_2) + U_3(e_3). \quad (22)$$

The functions U_2 and U_3 will be taken to be similar to the one-particle case, but with a stochastic ingredient, this stochasticity being totally uncorrelated in different spatial positions. We proceed as follows. We define a value e_0 (either e_{20} or e_{30} for e_2 or e_3) and define the corresponding U to be given by

$$U = 1 - \cos\left(\frac{(e - e_0)\pi}{\Delta}\right) \quad (23)$$

in the interval $|e - e_0| < \Delta$, where Δ is a random variable taken from a uniform distribution between 0.5 and 1. We monitor along the simulation the values of $e - e_0$ and compare against the value of Δ. Each time we detect $\pm(e - e_0) > \Delta$, a new value Δ_{new} is defined, and e_0 is redefined to $e_0 \pm (\Delta + \Delta_{\text{new}})$. In this form, we implement an independent stochastic disordered potential for e_2 and e_3 at each position in the sample.

Equations (20), (22), and (23) are numerically solved for a system with periodic boundary conditions, using a first-order Euler method that takes advantage of the transformation between real and Fourier space as convenient. A deformation rate $\dot{\gamma}$ is imposed on the e_2 variables by forcing the spatial average of e_2 to increase linearly in time as $\overline{e_2} = \dot{\gamma}t$. The corresponding stress σ is calculated as the temporal average of the instantaneous value $\sigma(t) = \lambda\dot{\gamma} - \overline{f_2}$. The volumetric stress is set to zero (except for the data in Fig. 7), namely $\overline{f_1} = 0$, by adjusting dynamically the average volume $\overline{e_1}$ according to

$$\kappa\dot{\overline{e_1}} = \overline{f_1}, \quad (24)$$

where $\kappa > 0$ is a "viscosity" parameter on e_1 (note that $f_1 > 0$ means an expansive stress). The dilatory effect that we are mostly interested in will depend on the fact that the temporal average of $\overline{e_1}$ will typically be different from zero.

IV. FLOW CURVES AND ORIENTATION OF SHEAR BANDS IN THE PRESENCE OF DILATANCY

The dilatancy effect in the PT model is the germ of a couple of interesting features that are found in the spatially extended model. In a spatially extended system, and in the absence of volume-shear coupling, correlated slips occur at 45° with respect to the principal axis of the stress tensor, as this is the orientation in which the maximum shear stress occurs. However, in the presence of volume-shear coupling, this angle changes [22,23]. We address this effect now.

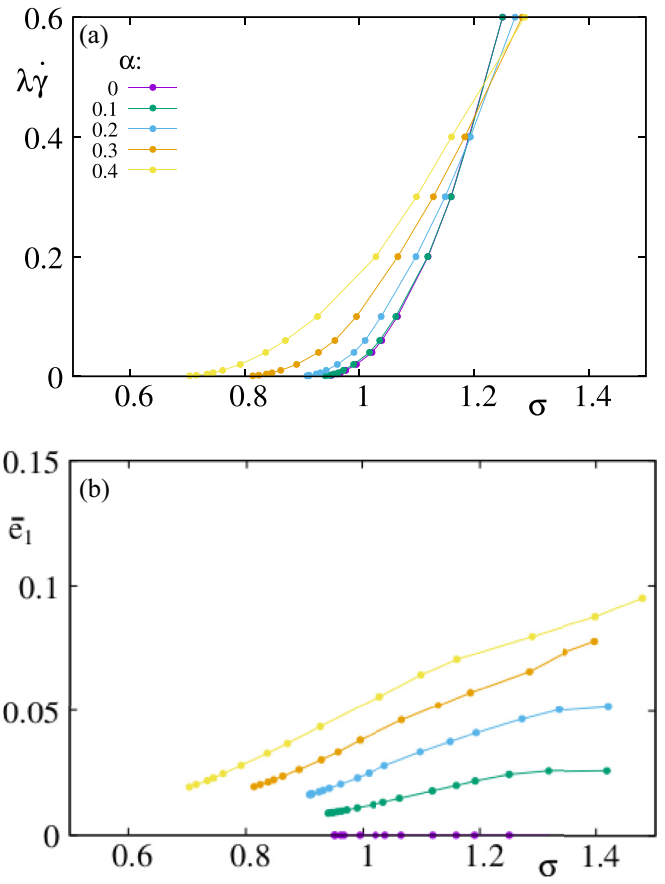

FIG. 4. (a) Flow-curves ($\dot{\gamma}$ vs σ) at different values of the volume-shear coupling parameter α, as indicated. (b) The corresponding curves for the average volume change. The qualitative behavior of the model is consistent with the results obtained in the one-particle case (Fig. 3).

Flow and volume curves for the spatially extended model are presented in Fig. 4. We observe in this case the same qualitative features obtained for the one-particle case (Fig. 3), namely a shift of curves to the left and an increase in system volume as α is increased. A more detailed inspection of the spatial distribution of deformation reveals a particular effect associated with a nonzero value of α. In Fig. 5 we see plots of accumulated strain e_2 in the system, at a relatively large value of $\lambda\dot{\gamma} = 0.1$, in systems with different values of α. In Fig. 5 the angle of correlation of plastic slips is clearly visible, and it is observed that this angle deviates from 45° when $\alpha \neq 0$. By calculating a correlation function on spatial configurations such as those in Fig. 5, the angle of maximum correlation can be determined with good precision. The result as a function of α is seen in Fig. 6. The angle is 45° in the case $\alpha = 0$, but it deviates from this value when $\alpha \neq 0$, the deviation being linear with α.

The orientation correlation of plastic activity (and ultimately the orientations of shear bands) with respect to principal stress directions is an important feature in many practical situations, so the reason for this reorientation is worth exploring in more detail. When $\alpha = 0$, the failure planes are determined by the condition of maximum shear stress, and this always occurs at 45° with respect to the

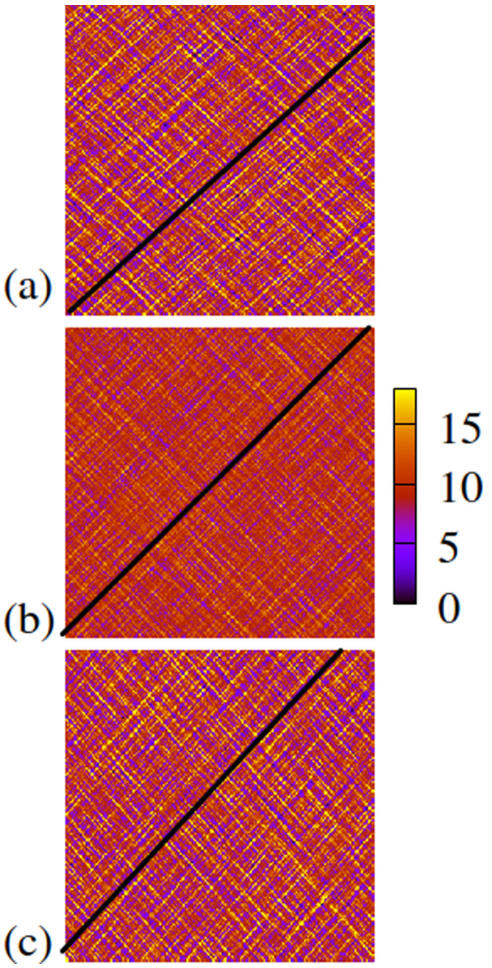

FIG. 5. Snapshots of accumulated deformation in the system in a fixed strain window at different values of the volume-shear coupling parameter: $\alpha = 0.2$ (a), 0 (b), and -0.2 (c). Note the change in the orientation of the slip lines (highlighted by the diagonal or off-diagonal straight black lines) as a function of α.

principal axis (in the present simulations they are the x and y axes, and we take $\sigma_x > \sigma_y$). However, if $\alpha \neq 0$ the stress normal to the failure plane plays a role, as a reduction in normal stress favors slip by reducing the critical stress. Therefore, there is a rotation of the slip planes with a normal that tends to align with the axis in which the compressive stress is minimum. The standard way to quantitatively calculate this rotation is the Mohr-Coulomb approach [2], which goes as follows. Considering potential slip planes appearing at an angle θ with respect to the x axis, the normal (σ_n) and shear (τ) stresses on these slip planes are given by

$$\sigma_n(\theta) = p - \sigma\cos(2\theta), \tag{25}$$

$$\tau(\theta) = \sigma\sin(2\theta), \tag{26}$$

where $p \equiv (\sigma_x + \sigma_y)/2$ and $\sigma \equiv (\sigma_x - \sigma_y)/2$. The Mohr-Coulomb theory relies on the assumption that a sample is in static mechanical equilibrium as long as the frictional stability condition

$$\tau(\theta) < \sigma_n(\theta)\mu + c \tag{27}$$

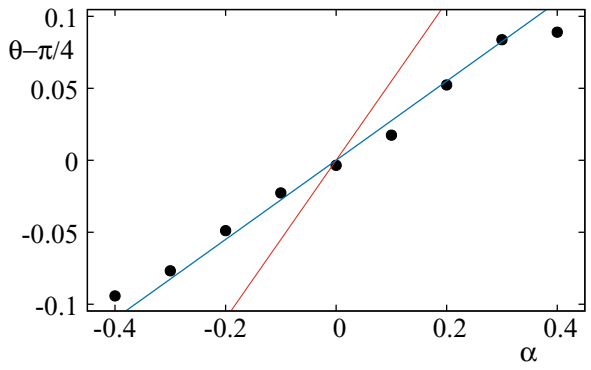

FIG. 6. Angle of maximum correlation between slips in the sample as a function of α. Dots are the measured values. The red line is the result of the Mohr Coulomb theory contained in Eq. (34). The blue line is the result of the theory in [22].

is satisfied for all θ, with μ and c being sample parameters named the internal friction coefficient and cohesion, respectively. Inserting Eqs. (25) and (26), the stability condition can be written as

$$[\sin(2\theta) + \mu\cos(2\theta)]\sigma < c + p\mu. \tag{28}$$

The Mohr-Coulomb criterion states that actual slips will occur at the angle θ for which this condition first becomes an equality. We emphasize that although this condition naturally emerges from the consideration of the Amontov-Coulomb static friction condition (27) between two sliding bodies, there is not a strong reason to believe that this will be strictly satisfied when considering the failure of a homogeneous material where no slip plane exists from the beginning. It is clear that failure according to the Mohr-Coulomb criterion occurs at a value of θ for which $[\sin(2\theta) + \mu\cos(2\theta)]$ is a minimum, predicting a slip angle given by

$$\theta = \tfrac{1}{2}\,\mathrm{atan}(\mu^{-1}). \tag{29}$$

Introducing the internal friction angle of the sample ϕ such that $\mu = \tan\phi$, θ can be written as

$$\theta = \pm\left(\frac{\pi}{4} - \frac{\phi}{2}\right). \tag{30}$$

To calculate the value of ϕ for a given sample, the *failure envelope* of the sample must be determined. By replacing Eq. (29) back into (28), it is obtained that failure (or yielding) occurs when

$$\sigma > \frac{c + p\mu}{\sqrt{1+\mu^2}} = c\cos(\phi) + p\sin(\phi). \tag{31}$$

Therefore, a determination of the stability region in the p, σ plane allows us to determine the values of ϕ and c, and calculate the slip angle θ.

A compressive stress p can be incorporated in our numerical scheme by modifying Eq. (24) to

$$\kappa\dot{\overline{e_1}} = (p + \overline{f_1}), \tag{32}$$

and the critical value of σ, namely σ_c, calculated as a function of p for different values α. The results (shown in Fig. 7) are

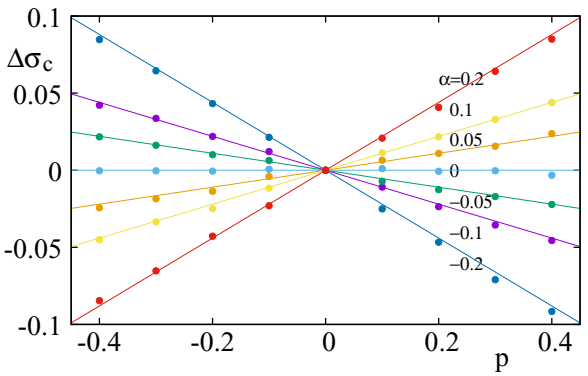

FIG. 7. Variation of the critical force $\Delta\sigma_c \equiv [\sigma_c(p) - \sigma_c(0)]$ as a function of the compressive stress p. Dots are the results of the simulations for different values of α. Lines are plots of the function $1.1\alpha p$, which provides a very good fitting of the numerical results.

compatible with a linear dependence of ϕ on α given by

$$\phi \simeq 1.1\alpha. \tag{33}$$

This expression can now be used in Eq. (30) to obtain

$$\theta \simeq \pm\left(\frac{\pi}{4} - 0.55\alpha\right), \tag{34}$$

which is the Mohr-Coulomb prediction for the angle of plastic slips in terms of the volume-shear coupling parameter α. This linear function is plotted in red on top of the numerical results in Fig. 6. It reproduces the linear trend of the numerical results, but it overestimates the numerical values by about a factor of 2. This kind of behavior goes in the same direction as experimental results, where it is observed also that Mohr-Coulomb theory overestimates the angle of shear bands with respect to $\pi/4$ [24].

The Mohr-Coulomb theory can be phenomenologically modified to try to fix experimental results more accurately, for instance introducing the dilatancy angle [24]. This could also be done here. However, we will proceed along a different line. Recently, Karimi and Barrat [22] have done a critical analysis of the correlation of plastic activity in yield stress materials, concluding also that the macroscopic Mohr-Coulomb criterion does not typically predict accurately the orientation of plastic correlations, or the macroscopic orientation of shear bands. They rely on an analysis in terms of the elastic coupling between plastic distortions and the *local* internal friction angle ϕ_0 [25] to conclude that the macroscopic slip line instabilities are expected to occur at an angle θ given by

$$\cos(2\theta) = \tfrac{1}{2}\sin(\phi_0) \tag{35}$$

or approximately

$$\theta \simeq \pm\left(\frac{\pi}{4} - \frac{\phi_0}{4}\right) \tag{36}$$

in cases in which ϕ_0 is not too large. The numerical factor of $1/4$ in the last term is very suggestive when this expression is compared to the Mohr-Coulomb one [Eq. (30)], and we remember the factor of 2 by which the Mohr-Coulomb criterion overestimates the numerically obtained values of θ (Fig. 6). Yet the angle θ_0 entering Eq. (36) is the *local* internal friction angle [22], which plays the same role as ϕ but for an elementary piece of the material, and it does not include the effects of the elastic interaction that are effectively incorporated in the macroscopic ϕ. We should find out whether ϕ and ϕ_0 differ appreciably or not. In our samples, the value of ϕ_0 is directly related to the shear volume coupling parameter α. We have measured this dependence by numerically finding the failure envelope now for a single element in the system, i.e., we ran the one-site model of Sec. II using the stochastic potential of the full model, and calculating the critical stress as a function of the normal stress. The slope of this dependence provides the value of $\sin(\phi_0)$. We have found that ϕ_0 can be adjusted as

$$\phi_0 \simeq 1.1\alpha. \tag{37}$$

Comparing with Eq. (33), we can conclude that in our model (and at least for the set of parameters that have been investigated), the local internal friction angle ϕ_0 coincides, within the numerical precision, with its macroscopic counterpart ϕ. Therefore, introducing (37) into expression (36), we obtain the values of θ as a function of α represented by the blue line in Fig. 6. They are a factor of 2 smaller than those provided by the Mohr-Coulomb theory, and they adjust very well to the orientation of numerical correlations observed for plastic slips in our simulations.

V. NONUNIFORM YIELDING CAUSED BY VOLUME-SHEAR COUPLING

An important phenomenon that may occur in the flowing of amorphous materials is localization of the deformation. In some cases (such as in metallic glasses; see the next section), this localization is a nonequilibrium phenomenon typically associated with the preparation of the sample. In other cases, this localization occurs in a steady-state evolution, and this is the situation that is addressed here. In Ref. [26], a stability analysis was performed for a flowing system that has, apart from the normal shear variables, additional scalar degrees of freedom taken to represent the concentration of solute molecules in the material. The analysis done is rather general, and it essentially applies also to the case in which the additional scalar variables can be considered to be the value of the local density in the system, as pointed out in [27]. Restricted to a two-dimensional situation appropriate to our case, the result of the analysis indicates that there are two different kinds of instabilities. In one of them, instability is purely mechanical, with the density degree of freedom playing no important role. The signature of such an instability is a flow curve that has a reentrance, namely a region in which stress diminishes as strain rate increases. This kind of instability is analogous to that producing phase separation in a one-component fluid, such as in the liquid-gas transition. In physical terms, this instability occurs in the following way. If a layer of the system that is shearing in a stationary way suffers a perturbation that increases its strain rate, then it would require less stress to maintain the new strain rate. But as the applied stress is kept fixed, this will produce an additional increase of strain rate, leading to an instability. This situation is known to occur, for instance, in cases in which there are aging mechanisms in the system [16,28–33]. It may thus happen that nonflowing regions maintain a well-aged state that is more rigid, and

therefore do not flow, while flowing regions, being unable to age sufficiently, have a lower critical stress and are maintained in a flowing state.

In addition to this kind of mechanical instability, it was found [26] that the coupling to the concentration degree of freedom can produce a breaking of the uniform flow, even in the absence of any strong feature of the flow curve. This instability is qualitatively understood in the following way [10,34,35]. If on an originally uniform yielding state a fluctuation in some part of the sample produces an increase in strain rate, then that part of the system will also experience an expansion, which in turn produces a decrease in the effective viscosity and a further increase in the strain rate. This process can eventually lead to an instability, which, however, does not manifest clearly in the form of the flow curve of the system.

We have observed this kind of instability in the present model in the case in which α is large enough. The numerical evidence is contained in Fig. 8. There in the left column we observe plots of the accumulated deformation in the system in a rather long time window at a constant value of $\lambda\dot{\gamma} = 0.1$, and for different values of α. For low α ($\alpha \lesssim 0.2$) the deformation is uniform, whereas for larger α we clearly see that there are regions in the system that have not yielded at all, showing the nonuniform yielding in this case. The instantaneous values of the volume variable e_1 across the system (right column in Fig. 8) show also a clear correlation with the deformation in the large α cases, with the sample flowing in regions in which the local volume is well above the average value. Stuck regions instead correspond to compressed sample regions, with values of e_1 below the average. Notice that in spite of the spatial localization observed, the corresponding flow curves (which are precisely those in Fig. 4) are monotonic.

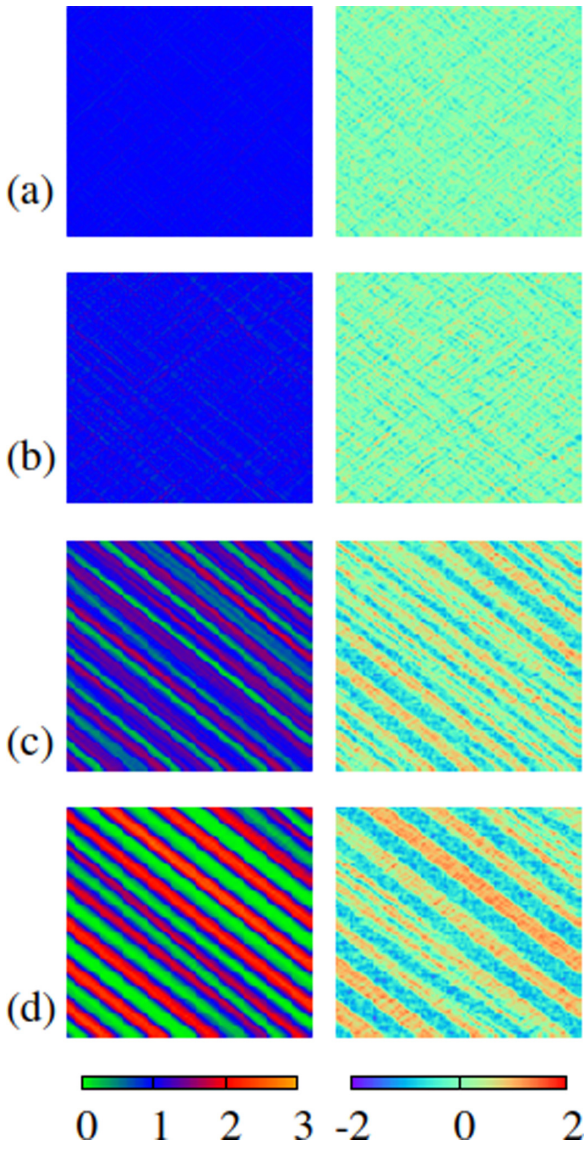

FIG. 8. Accumulated strain deformation (left column, the scale value 1 corresponds to the nominal average deformation in all cases) and instantaneous values of e_1 (right column) in simulations at the same value of $\lambda\dot{\gamma} = 0.1$, in systems with different values of shear-volume coupling parameter α, namely $\alpha = 0.1$ (a), 0.2 (b), 0.3 (c), and 0.4 (d) (system size is 128×128). The long-term deformation is uniform in the first two cases, but is inhomogeneous in the last two.

VI. VOLUME-SHEAR COUPLING IN ANNEALED SAMPLES. THE CASE OF METALLIC GLASSES

The effects of volume-shear coupling that have been discussed so far all correspond to situations of dynamical equilibrium in the system, or in other words, they all describe stationary situations. There are other situation, however, in which we are interested in transient (although probably long-lived) properties of the system. In many cases, this occurs when an experiment is done on a sample prepared by some ad-hoc protocol that leaves it in an out-of-equilibrium configuration. To be concrete, we want to refer to the case of metallic glasses [12–15]. They are usually prepared by annealing from a melt, and their configuration cannot by any means be considered as an equilibrium one. When metallic glass is submitted to an external load, the appearance of a shear band is a highly nonequilibrium process. Yet the kind of models we have presented can be used to model this scenario, and in particular the effect of volume fluctuations on the behavior of this kind of material.

The key to mimic the behavior of a metallic glass under shear is to start with an initial configuration that appropriately incorporates the annealed nature of the experimental initial state. In our model, we can produce a starting configuration that is more stable than the stationary one after long deformation by adjusting the local disorder potentials at different sites [16]. The local potentials are characterized by the values of e_{20} and e_{30}, defining the local equilibrium strain, and the corresponding values of Δ measuring the extent of the corresponding basin. In stationary situations such as those considered so far, the values of e_0 have some dynamically generated dispersion, and Δ is randomly chosen from a uniform distribution between 0.5 and 1.0. We can construct a more stable starting sample by appropriately modifying e_0 and/or Δ.

The possibility that is implemented here is to take a steady-state configuration obtained after a long run with a constant $\dot{\gamma}$, and setting the values of e_{20} or e_{30} to be equal to the instantaneous values of e_2 or e_3. This generates [according

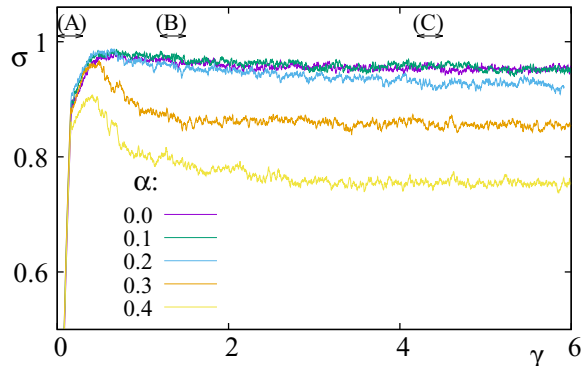

FIG. 9. Stress-strain curves (using $\lambda\dot{\gamma} = 0.001$) in samples with different values of α as indicated, after an annealing in the initial state, as described in the text. All curves display a stress overshoot above the asymptotic values, but the effect is much stronger in samples with large α.

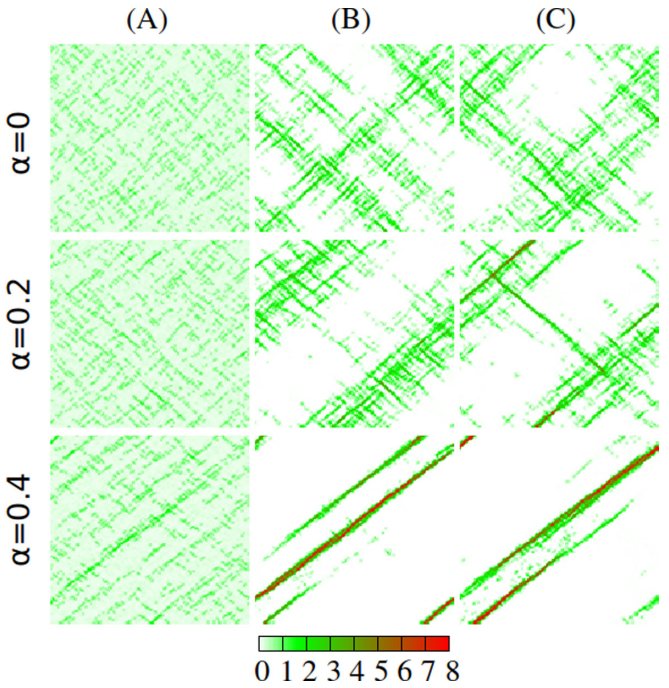

FIG. 10. Accumulated spatial distribution of strain in the three strain windows indicated in Fig. 9, for three different values of α. Although for all values of α we observe strain localization, the effect for larger α produces a much narrower shear band.

to Eq. (23)] a state that is much more relaxed than the initial steady state. This new configuration is taken as the initial state onto which a finite strain rate $\dot{\gamma}$ is applied, and the dynamics is followed exactly as before.

The results obtained are shown in Fig. 9 for systems with different intensities of volume-shear coupling. All curves in Fig. 9 display a stress overshoot that is the hallmark of annealed samples that are more stable than the asymptotic steady state. Yet we see that the amplitude of the stress overshoot is much more pronounced in samples with a larger value of α. To have a deeper understanding of the effect of α, we must investigate the local distribution of deformation in the samples. In Fig. 9 we have indicated three strain windows, labeled (A), (B), and (C). The local distribution of accumulated strain in each of these windows is indicated in Fig. 10 for three different values of α, namely $\alpha = 0, 0.2, 0.4$.

The case $\alpha = 0$ serves as a reference, and it is similar to that studied in Ref. [16]. We emphasize that even in this case, an overshoot is observed in the stress-strain curve (Fig. 9). In the strain window (A), when stress is still increasing in the system, we observe rather isolated plastic events that do not yet organize across the sample. In strain windows (B) and (C) instead, when the stress peak has been overpassed, the plastic strain is localized in a spatial region that can be termed a shear band. The reason for this behavior is that in the shear band the system was forced to escape from the initial annealed state, and its critical stress is now lower than in the still annealed part, which is nonflowing. This stabilizes the shear band in the system. This shear band widens as $\sim\gamma^{1/2}$ when strain is increased [36–38]. Notice that the strain localization at $\alpha = 0$ is not observable in the distribution of the volume variable e_1 [Fig. 11(a)].

The case of a finite shear-volume coupling ($\alpha > 0$) produces some quantitative differences and also some qualitative new phenomena. First of all, in Fig. 9 we clearly see how the increasing part of the stress-strain curve is not very dependent on the value of α, and in fact the spatial distribution of the deformation in strain window (A) shows a rather uniform deformation distribution independently of α. However, after the stress peak is overcome, the stress decrease is much larger in samples with large α. The analysis of the spatial distribution of deformation reveals that the accumulated strain at finite α shows a stronger tendency to become more localized, and a much weaker tendency to widen as strain increases. Most remarkably, for values of α where we had previously observed an instability of the homogeneous deformation situation ($\alpha \gtrsim 0.2$; see Fig. 8), we now observe that only a very thin shear band is activated in the system, with all the rest remaining in a rigid configuration. This is very clear in the plots corresponding to $\alpha = 0.4$ in Fig. 10. Notice that as the shear band does not run exactly along the diagonal (see Sec. III), and because of the periodic boundary conditions, there are some "mirror images" of the shear band, giving the impression of a few different shear bands in the system. The very thin shear bands observed in the presence of a strong volume-shear coupling allow us to speculate that volume-shear coupling is also an important ingredient in the dynamics of metallic glasses, where failure by the nucleation of thin shear bands is regularly observed.

We think the most remarkable effect of a finite α manifests in the spatial distribution of the e_1 variable (Fig. 11). While for $\alpha = 0$ we did not have any clue of the strain localization from the distribution of e_1, in the finite α case, particularly when $\alpha \gtrsim 0.2$, this is not so. In fact, in Fig. 11(c) we clearly observe that the localization of the shear band corresponds to a region where the system is expanded (therefore facilitating the shearing of the system in this region). We emphasize that if we stop increasing the strain in the system, or even if strain is reduced as necessary to reach a state of zero stress, the spatial distribution of e_1 remains essentially at the metastable configuration shown in Fig. 11. Therefore, the localization of

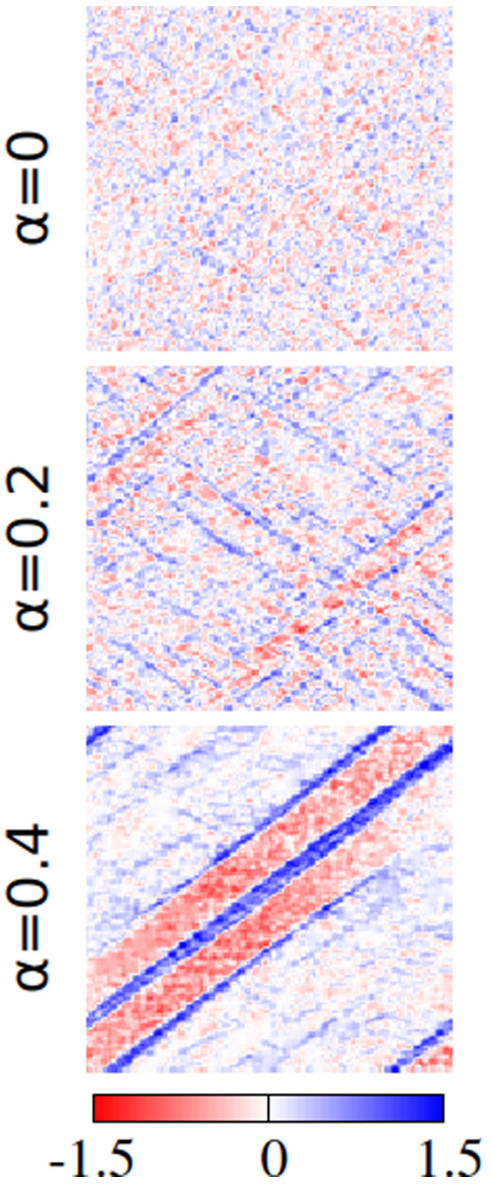

FIG. 11. Instantaneous distribution of the volumetric e_1 variable, right after the time window (C), for the three different values of α presented in Fig. 10. The position of the shear band in the system can be inferred from the distribution of e_1 in the case in which α is large.

the shear band where the system has yielded can be evaluated after the full process has taken place by localizing the regions of the sample that are expanded with respect to the starting configuration.

VII. SUMMARY AND CONCLUSIONS

In this work, we have introduced a mesoscopic model for the yielding behavior of amorphous materials incorporating the possibility of volume-shear coupling. This ingredient is acknowledged to have important experimental consequences, but it has only rarely [22] been previously considered in numerical models of the yielding transition. Volume-shear coupling produces a number of effects in the phenomenology of yield stress materials. It generates a change in the direction of the shear bands in the system. Our numerical simulations clearly show this angular deviation. We have applied the classical Mohr-Coulomb approach and the theory in Ref. [22] to predict the deviation, and we find that the prediction in [22] nicely fits our numerical results, whereas the Mohr-Coulomb theory tends to overestimate the reorientation effect. Also, we have observed that when the volume-shear coupling is strong enough, there is a tendency of the system to generate a nonuniform deformation. In this case, there are regions that become more expanded and therefore yield more easily, while others remain in a more compact configuration and do not yield at all. Finally, we have briefly discussed the effect of volume-shear coupling in cases in which the sample is initially annealed to obtain a starting configuration that is more stable than the asymptotic configuration that appears as a stationary state after a very long deformation time. This situation is particularly adapted to the phenomenology of metallic glasses. Now, when the sample is strained, the stress in the system develops a peak before smoothly decaying to the asymptotic stress value. The case of no volume shear-coupling has been studied in previous works [16,37,39] and it was observed that after the strain corresponding to the stress maximum is exceeded, the deformation in the sample localizes in a shear band. This band progressively widens with further deformation as discussed in Refs. [36,38]. Now in the case in which there is volume-shear coupling, particularly when this is large, we observe that the shear band that appears in the system is very thin, and we do not detect clearly that it widens as deformation proceeds. We observed that in the region of this thin band the system is expanded, and this expansion remains even if deformation is stopped and stress relaxes back to zero. All these findings point to the utility of the present kind of model in the study of shear stress materials for which shear-volume coupling is important.

ACKNOWLEDGMENT

I thank Ezequiel Ferrero for helpful stimulating discussions, and Kamran Karimi for bringing to my attention the theory in Ref. [22].

[1] O. Reynolds, On the dilatancy of media composed of rigid particles in contact, with experimental illustrations, London, Edinburgh, Dublin Philos. Mag. J. Sci. **20**, 469 (1885).

[2] R. M. Nedderman, *Statics and Kinematics of Granular Materials* (Cambridge University Press, Cambridge, 1992).

[3] W. E. H. Culling, Soil creep and the development of hillside slopes, J. Geol. **71**, 127 (1963).

[4] Dietrich, W. E. Dietrich, D. G. Bellugi, L. S. Sklar, J. D. Stock, A. M. Heimsath, and J. J. Roering, Geomorphic transport laws for predicting landscape form and dynamics, Geophys. Monogr. Am. Geophys. Union **135**, 103 (2003).

[5] J. J. Roering, J. W. Kirchner, and W. E. Dietrich, Hillslope evolution by nonlinear, slope-dependent transport: Steady state morphology and equilibrium adjustment timescales, J. Geophys. Res.: Solid Earth **106**, 16499 (2001).

[6] D. J. Jerolmack and K. E. Daniels, Viewing Earth's surface as a soft-matter landscape, Nat. Rev. Phys. **1**, 716 (2019).

[7] D. Bonn, M. M. Denn, L. Berthier, T. Divoux, and S. Manneville, Yield stress materials in soft condensed matter, Rev. Mod. Phys. **89**, 035005 (2017).

[8] A. Nicolas, E. E. Ferrero, K. Martens, and J.-L. Barrat, Deformation and flow of amorphous solids: Insights from elastoplastic models, Rev. Mod. Phys. **90**, 045006 (2018).

[9] G. Ovarlez, S. Cohen-Addad, K. Krishan, J. Goyon, and P. Coussot, On the existence of a simple yield stress fluid behavior, J. Non-Newtonian Fluid Mech. **193**, 68 (2013).

[10] R. Besseling, L. Isa, P. Ballesta, G. Petekidis, M. E. Cates, and W. C. K. Poon, Shear Banding and Flow-Concentration Coupling in Colloidal Glasses, Phys. Rev. Lett. **105**, 268301 (2010).

[11] P. Coussot, Yield stress fluid flows: A review of experimental data, J. Non-Newtonian Fluid Mech. **211**, 31 (2014).

[12] C. Tang, H. Peng, Y. Chen, and M. Ferry, Formation and dilatation of shear bands in a Cu-Zr metallic glass: A free volume perspective, J. Appl. Phys. **120**, 235101 (2016).

[13] A. L. Greer, Y. Q. Cheng, and E. Ma, Shear bands in metallic glasses, Mater. Sci. Eng. R **74**, 71 (2013).

[14] S. Ogata, F. Shimizu, J. Li, M. Wakeda, and Y. Shibutani, Atomistic simulation of shear localization in Cu-Zr bulk metallic glass, Intermetallics **14**, 1033 (2006).

[15] C. Zhong, H. Zhang, Q. P. Cao, X. D. Wang, D. X. Zhang, U. Ramamurty, and J. Z. Jiang, Deformation behavior of metallic glasses with shear band like atomic structure: A molecular dynamics study, Sci. Rep. **6**, 30935 (2016).

[16] E. A. Jagla, Strain localization driven by structural relaxation in sheared amorphous solids, Phys. Rev. E **76**, 046119 (2007).

[17] I. Fernández Aguirre and E. A. Jagla, Critical exponents of the yielding transition of amorphous solids, Phys. Rev. E **98**, 013002 (2018).

[18] E. E. Ferrero and E. A. Jagla, Criticality in elastoplastic models of amorphous solids with stress-dependent yielding rates, Soft Matter **15**, 9041 (2019).

[19] V. L. Popov and J. A. T. Gray, Prandtl-Tomlinson model: History and applications in friction, plasticity, and nanotechnologies, ZAMM. Z. Angew. Math. Mech. **92**, 683 (2012).

[20] E. A. Jagla, Tensorial description of the plasticity of amorphous composites, Phys. Rev. E **101**, 043004 (2020).

[21] D. Chandrasekharaiah and L. Debnath, *Continuum Mechanics* (Academic Press, San Diego, 1994).

[22] K. Karimi and J.-L. Barrat, Correlation and shear bands in a plastically deformed granular medium, Sci. Rep. **8**, 4021 (2018).

[23] J. Ashwin, O. Gendelman, I. Procaccia, and C. Shor, Yield-strain and shear-band direction in amorphous solids under two-dimensional uniaxial loading, Phys. Rev. E **88**, 022310 (2013).

[24] J. Bardet, A comprehensive review of strain localization in elastoplastic soils, Comput. Geotech. **10**, 163 (1990).

[25] Note that our variables ϕ and ϕ_0 are notated in Ref. [22] as ϕ_r and ϕ, respectively. Also in Ref. [22], an effect of "dilatancy" on the relation between θ and the internal friction angle is predicted. Although our shear volume coupling mechanism induces dilatancy of the sample, we think the effect discussed in [22] does not apply to the results in this section, because here the sample is dilated permanently and uniformly.

[26] V. Schmitt, C. M. Marques, and F. Lequeux, Shear-induced phase separation of complex fluids: The role of flow-concentration coupling, Phys. Rev. E **52**, 4009 (1995).

[27] M. Gross and F. Varnik, Shear-density coupling for a compressible single-component yield-stress fluid, Soft Matter **14**, 4577 (2018).

[28] G. Picard, A. Ajdari, L. Bocquet, and F. Lequeux, Simple model for heterogeneous flows of yield stress fluids, Phys. Rev. E **66**, 051501 (2002).

[29] P. D. Olmsted, Perspectives on shear banding in complex fluids, Rheol. Acta **47**, 283 (2008).

[30] T. Divoux, M. A. Fardin, S. Manneville, and S. Lerouge, Shear banding of complex fluids, Annu. Rev. Fluid Mech. **48**, 81 (2016).

[31] P. Coussot, Q. D. Nguyen, H. T. Huynh, and D. Bonn, Avalanche Behavior in Yield Stress Fluids, Phys. Rev. Lett. **88**, 175501 (2002).

[32] A. Mujumdar, A. N. Beris, and B. Metzner, Transient phenomena in thixotropic systems, J. Non-Newtonian Fluid Mech. **102**, 157 (2002).

[33] K. Martens, L. Bocquet, and J.-L. Barrat, Spontaneous formation of permanent shear bands in a mesoscopic model of flowing disordered matter, Soft Matter **8**, 4197 (2012).

[34] A. Fall, F. Bertrand, G. Ovarlez, and D. Bonn, Yield Stress and Shear Banding in Granular Suspensions, Phys. Rev. Lett. **103**, 178301 (2009).

[35] G. Ovarlez, F. Bertrand, and S. Rodts, Local determination of the constitutive law of a dense suspension of noncolloidal particles through magnetic resonance imaging, J. Rheol. **50**, 259 (2006).

[36] E. A. Jagla, Shear band dynamics from a mesoscopic modeling of plasticity, J. Stat. Mech. (2010) P12025.

[37] Y. Shi, M. B. Katz, H. Li, and M. L. Falk, Evaluation of the Disorder Temperature and Free-Volume Formalisms via Simulations of Shear Banding in Amorphous Solids, Phys. Rev. Lett. **98**, 185505 (2007).

[38] D. D. Alix-Williams and M. L. Falk, Shear band broadening in simulated glasses, Phys. Rev. E **98**, 053002 (2018).

[39] D. Vandembroucq and S. Roux, Mechanical noise dependent aging and shear banding behavior of a mesoscopic model of amorphous plasticity, Phys. Rev. B **84**, 134210 (2011).